Research Square

Preprints are preliminary reports that have not undergone peer review.
They should not be considered conclusive, used to inform clinical practice,
or referenced by the media as validated information.

Stratospheric enhancement of tropical cyclone high-level warm cores

Andrea Davin

a.davin@campus.unimib.it

University of Milano-Bicocca

Giousef Alexandros Charinti

Institute of Science and Technology Austria

Caroline Muller

Institute of Science and Technology Austria

Claudia Pasquero

University of Milano-Bicocca

Short Report

Keywords:

Posted Date: November 16th, 2026

DOI: https://doi.org/10.21203/rs.3.rs-11477246/v1

License: This work is licensed under a Creative Commons Attribution 4.0 International License.
Read Full License

Additional Declarations: No competing interests reported.

Stratospheric enhancement of tropical cyclone high-level warm cores

Andrea Davin*[1], Giousef Alexandros Charinti[2], Caroline Muller[2], Andrea Polesello[2], and Claudia Pasquero[1]

[1]Department of Earth and Environmental Sciences, University of Milan-Bicocca, Milan, Italy
[2]Institute of Science and Technology Austria, Klosterneuburg, Austria

October 27, 2026

Abstract

Mature tropical cyclones are characterized by warm cores. Reanalysis data show that stratospheric intrusions can intensify these cores in the upper troposphere, forming stratospheric-enhanced high-level warm cores. Their frequency increases with storm strength, despite minimal dependence on potential intensity. They preferentially form in storms with longer intensification periods, weaker wind shear, and greater coastal distance, suggesting they are less likely when unfavourable conditions keep cyclones below their upper thermodynamic limit.

1 Main text

Despite steady improvements in the forecasting of tropical cyclone (TC) tracks, the prediction of their intensity remains a considerably harder problem [1]. Intensity changes respond both to the large-scale environment, through factors such as sea-surface temperature (SST) [2] and vertical wind shear (VWS) [3], and to internal processes that can operate even under steady environmental conditions, including eyewall replacement cycles [4] and the interplay between static and inertial stability [5].

Among internal processes, the thermal structure of the storm core has drawn attention since the seminal work of [6], who showed that it can indicate the evolutionary phase of a TC. The defining thermodynamic feature of a mature TC is a mid-level warm core, a region of positive temperature anomaly in the eye. Its air is first warmed by latent heat released in eyewall convective updrafts, and then further warmed by adiabatic compression as it subsides. Mature storms are inertially stable vortices, thus lateral displacements of air within their core are hindered. When subsiding air heats inside the core, the heat remains confined in this region instead of being dispersed by gravity waves [5].

Both observations [7] and numerical simulations [8–14] show how the positive temperature anomaly can be amplified at upper levels by the intrusion of lower-stratospheric air into the troposphere. As air of stratospheric origin subsides, adiabatic compression warms it beyond the temperature of the surrounding air, owing to its higher potential temperature, producing a body of anomalously

*Corresponding author: a.davin@campus.unimib.it

warm air referred to as a High-level Warm Core (HWC), distinct from the mid-level warm core of tropospheric air [8, 10, 14].

Stratospheric air intrusions in the troposphere are often due to tropopause folding [15]. In intense TCs, however, overshooting convection above the tropopause can trigger robust two-way exchanges between troposphere and stratosphere, in both the inner region and the outer rain bands [10, 13, 16, 17]. The presence of those exchanges in TCs has been extensively documented in studies of air compositional changes near the tropopause from satellite observations: water vapor and ozone anomalies are consistent with the effects of injection of ice particles in the lower stratosphere [16, 18, 19] and with detrainment of stratospheric ozone [20, 21].

The role of HWCs in intensity evolution is not entirely settled. A large part of the literature on this topic has focused on how warmer air aloft lowers the hydrostatic surface pressure, thereby favouring intensification [8, 9, 11]. However, the same mechanism, especially when the warm anomaly is not confined to the eye but extends to larger distances from the center, can be held accountable for the stabilisation of the air column aloft, as warming at upper levels inhibits deep convection, thus contributing to weakening [22, 23]. Recent high-resolution simulations suggest that these two effects are not necessarily mutually exclusive, but rather act on different timescales, so that a HWC may first strengthen a cyclone and later limit its intensity [12, 14].

Most of these results come from individual case studies or from convection-permitting, cloud-resolving simulations of single storms [8–10, 12, 13]. Although the role of HWC on TC evolution has been documented also in realistic fine-scale simulations of the atmosphere [14], it remains unclear how common warm stratospheric intrusions are across the global TC population, whether their occurrence depends on TC properties such as storm intensity, and which environmental conditions generally favour their development. A systematic, data-driven characterisation over a large sample of storms is still missing.

In this work we address this gap through a comprehensive analysis of stratospheric intrusions in TCs over the period 1981-2020. We combine best-track positions from the International Best Track Archive for Climate Stewardship (IBTrACS; [24]) with the environmental fields of the ERA5 reanalysis dataset [25].

Out of the 2112 TCs analysed, 966 were labelled as "stratospheric-enhanced HWC developing storms" (hereafter "SE-HWC-storms") and the remaining 1146 "non-SE-HWC-storms". The classification is based on a newly introduced "Stratospheric Intrusion Index" (SII, see Sec 2.2 and Fig. 1). This classifier, based on the difference between equivalent potential temperature (θ_e) at 200 hPa and at the surface, is conceptually related to similar HWC metrics proposed by [8, 13, 14]. The distribution of the maximum upward mass flow rate at 200 hPa (F_{max}) reported in Fig. 1d supports this classification, showing that air mass vertical exchanges at the top of the troposphere become stronger in SE-HWC-storms compared to non-SE-HWC-storms, as expected.

The fraction of cyclones with a stratospheric intrusion depends on the intensity of the storm (v_{max}, Fig. 2a), ranging from about 10% for weak tropical storms to 80% for cyclones in category 5 of the Saffir-Simpson scale. This dependence on cyclone strength is not driven by systematic differences in the thermodynamical factors that determine the theoretical upper limit for cyclone intensity, such as pre-storm SST, air-sea enthalpy difference (Δk), and outflow temperature (T_o) (see Supplementary S4). These variables are statistically similar between the two classes, with the exception of SST, which is slightly lower for SE-HWC-storms (see Supplementary S3 and S4). This reduced SST is reflected in a slightly, though not significantly, lower potential intensity (PI, see Methods section 2.4) in SE-HWC-storms (Fig. 3a). SE-HWC-storms occurrence is overall fairly independent of storm PI, taken here as the maximum value along the cyclone track (Fig. 2b).

The fact that SE-HWC-storms attain an intensity much closer to PI than non-SE-HWC-storms (Fig. 3b), suggests a direct link between the strength of the cyclone and the intrusion of stratospheric air rather than a dependence on near surface properties or static stability. In

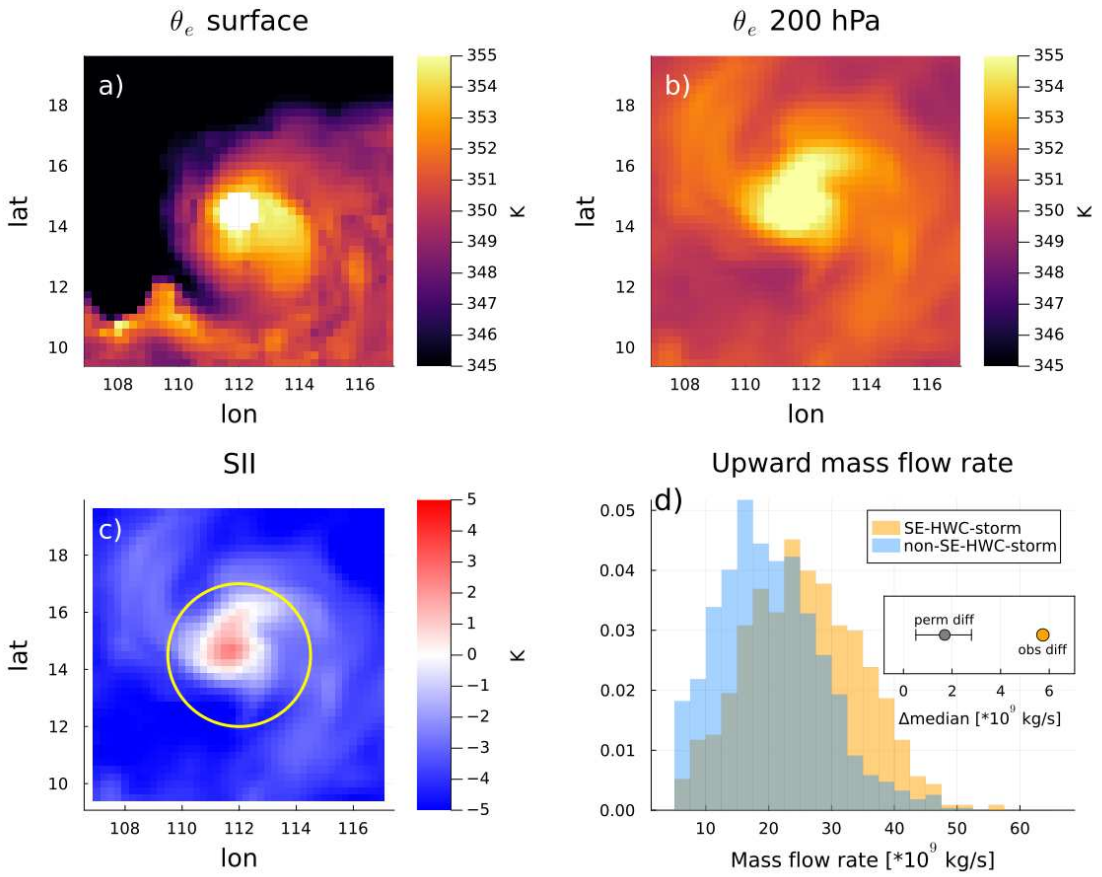


Figure 1: (a) Surface equivalent potential temperature for the TC "Kai-Tak" (2005) over the Western Pacific and (b) at 200 hPa. (c) The stratospheric intrusion index, SII, i.e. the 200 hPa θ_e anomaly relative to the surface maximum for the same snapshots. (d) Normalized distributions of the along-track maximum upward mass flow rate F_{max} at 200 hPa for the two classes of cyclones. The inset reports the result of the statistical test described in Section 2.4.

fact, v_{max} in 75% of non-SE-HWC-storms does not reach half of the PI, whereas more than 2/3 SE-HWC-storms overcome this threshold.

It has already been highlighted that SE-HWC-cyclones are characterized by a stronger peak upward mass transport near the tropopause. Further investigation, described in Section 2.4 and summarized in Table 1, reveals that this is associated with a stronger vertical flux and a larger updraft area (Supplementary S5). Considering that the average time tendency of the upward mass flow rate up to F_{max} is similar in both cyclone classes (Fig. 4a) and that the initial F at the time TCs attain tropical storm intensity (TS time) is similar between classes (Supplementary S5), the key difference is the duration of the intensification phase, which is significantly longer for SE-HWC-storms (Fig. 4b). The intensification period, defined as the time from tropical storm intensity to peak intensity, averages about 1.5 days for non-SE-HWC and 3.5 days for SE-HWC-storms. A similar difference holds even within each TC category (Supplementary S6), suggesting that both intensity and duration of the intensification phase play a role in the formation of SE-HWC. Contributions from different TC detrimental effects are present and can explain this difference: SE-HWC-storms experience on average weaker high-level VWS than non-SE-HWC ones, are embedded

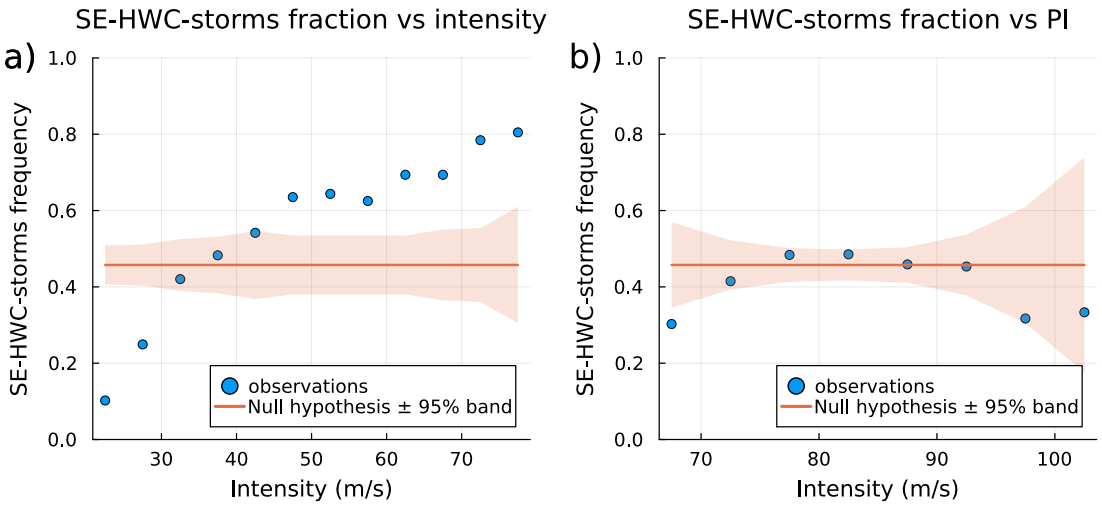


Figure 2: (a) Frequency of SE-HWC-storms as a function of v_{max}, tested against the null hypothesis of a constant probability of occurrence across intensity bins. (b) The same plot as a function of PI.

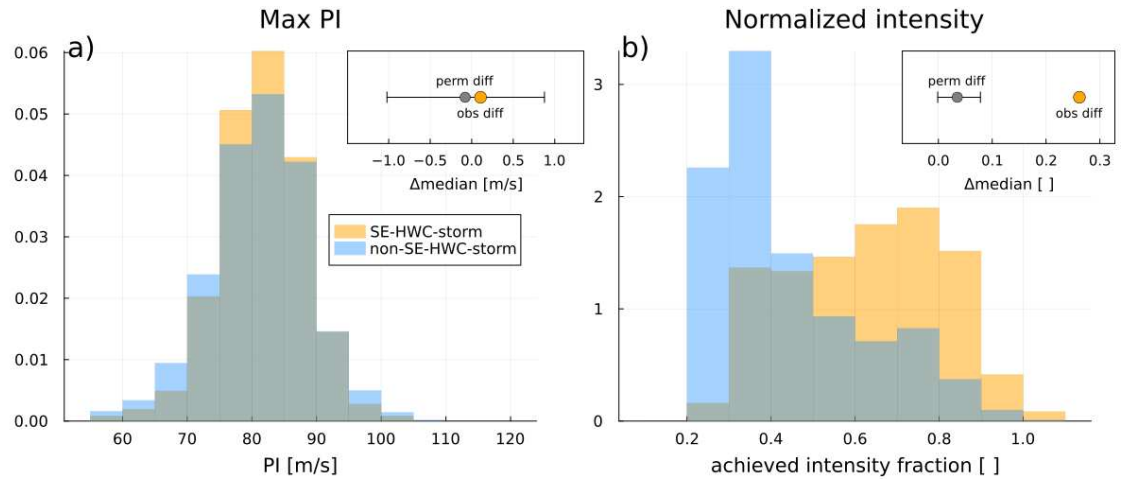


Figure 3: Normalised distributions of the SE-HWC-storms (yellow) and non-SE-HWC-storms (blue) population for (a) PI and (b) normalized intensity. The inset within each plot displays the statistical significance of the difference of the median value of each variable between the two classes, tested against the null distribution obtained with permutations (see Section 2.4).

in an environment with larger mid-level moisture and are further from coastlines (Fig. 5). All those differences are statistically significant and refer to characteristics that are known to be associated with processes that weaken or inhibit intensification. Strong vertical wind shear disrupts the vertical alignment of the storm and ventilates the warm core, mid-level dry air intrusions suppress convection via evaporative cooling and create downdrafts [26], and interactions with land cut off moisture and heat sources.

These results indicate that SE-HWC-storms reach higher intensities because they are less affected by detrimental processes and can thus intensify for longer times and attain strengths closer

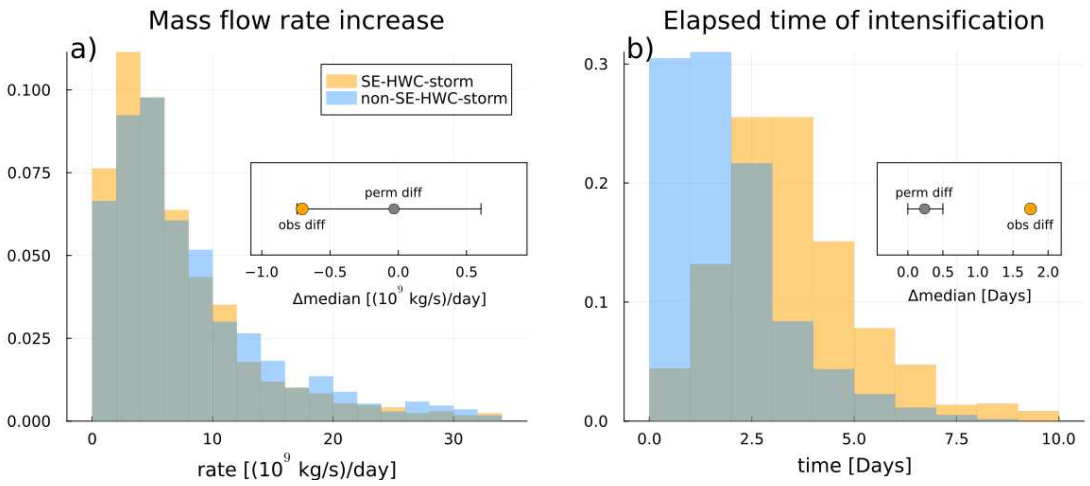


Figure 4: As Fig. 3 for (a) near tropopause upward mass flow rate tendency, (b) elapsed intensification time.

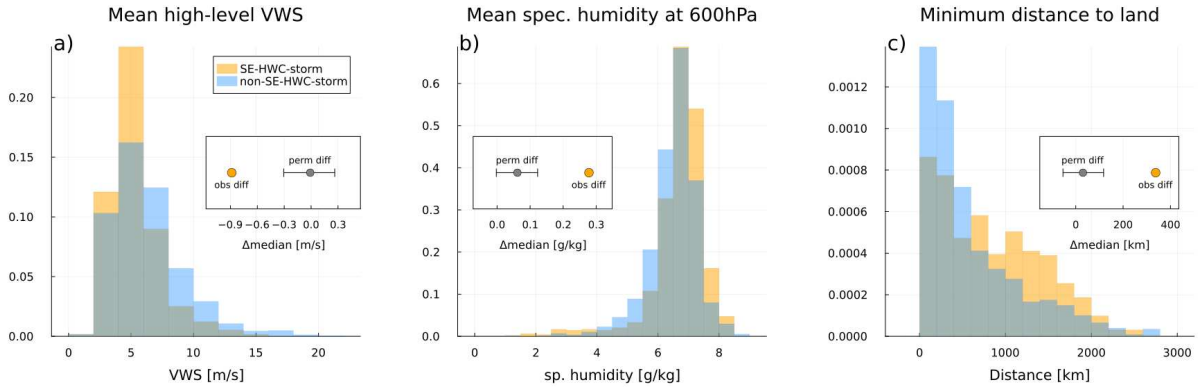


Figure 5: As Fig. 3 for (a) the high-level VWS, (b) specific humidity at 600 hPa and (c) distance to land at peak intensity.

to their PI, rather than because of a systematically more favourable pre-storm thermodynamic environment. The longer intensification period also increases the upward mass flow rate near the tropopause, and thus exchanges between troposphere and stratosphere, allowing the formation of the upper-level warm core.

Having been previously documented only in case studies [7–10, 27], the frequency of occurrence of SE-HWCs was not well established. In this study we document for the first time that tropical storms have a probability of 20% of developing a SE-HWC, and that perturbations reaching hurricane intensity are associated with SE-HWCs in more than 50% of cases. The dependence on intensity is consistent with previous results that showed that the magnitude of the stratospheric-tropospheric exchanges strengthens with increasing TC intensity [19, 21, 28].

These results have been obtained identifying stratospheric intrusions based on an equivalent potential temperature framework in the ERA5 reanalysis product, whose representation of the lower stratosphere is typically considered reliable for large-scale dynamics and temperature [25]. It is worth noting that ERA5 has a known systematic cold error for the 2000-2006 period [29], whose effects on the present analysis would be to reduce the magnitude of upper level warming in presence of stratospheric intrusions. This might lead to missing the detection of some SE-HWC in the affected years.

While for non-SE-HWC-storms, external factors such as wind shear, interaction with land, and mid-level dryness limit their intensity, for SE-HWC-storms those detrimental effects are certainly less important. This allows, as discussed, for the higher normalized intensity reached by SE-HWC-storms. It also opens the question of what processes prevent them from reaching their potential intensity. The possibility that the high-level warm cores become important for the subsequent ceiling of intensity and even the weakening of the cyclone remains open, and further studies will be needed to link the appearance of the SE-HWC to the change in intensification rate. Having demonstrated that SE-HWCs are a very common feature of intense cyclones, this investigation could be done on a relatively large cyclone dataset.

2 Methods

In the following we describe the selection criteria for the TC dataset construction, define the "Stratospheric Intrusion Index" (SII), which is then used to classify cyclones into SE-HWC-storms and non-SE-HWC-storms, and finally describe the analysis methods for the dynamical properties of the TCs and the thermodynamical ones for the environments where they developed.

2.1 Dataset

Tropical cyclone tracks and characteristics (e.g., intensity or distance to land) were extracted from IBTrACS, while the environmental variables come from the ERA5 reanalysis dataset at full horizontal resolution (0.25°). Both datasets were sampled at a 6-hourly time resolution. To match the TC location reported in IBTrACS with the ERA5 regular grid, the storm locations were used as a starting point to find the closest sea-level pressure (SLP) minimum within a $2°\times2°$ box in ERA5. Given the known difficulties of reanalyses in representing TCs [30], we analyse these environmental properties under pre-storm (i.e., 3 days before) conditions, except where specified otherwise.

TCs that made landfall or underwent extratropical transition within one day of the time of peak intensity were excluded from the analysis; the reason for this exclusion is clarified in Section 2.2. A total of 2112 storms, formed between the years 1981-2020, composed the population used in the statistical analysis presented in the paper.

2.2 Stratospheric Intrusion Index

Equivalent potential temperature θ_e is approximately conserved in moist convection and is largest in the stratosphere; it can therefore be used as an effective tracer of stratospheric air that has descended into the troposphere [12, 14, 31]. In deep convection, boundary-layer air rising adiabatically or entraining air from the surrounding troposphere cannot produce upper-level θ_e values that exceed those near the surface, so a positive θ_e anomaly aloft with respect to the boundary layer can be interpreted as a signature of stratospheric intrusion.

On this basis, we introduce the Stratospheric Intrusion Index (SII), obtained by comparing the upper-level (200 hPa) tropospheric θ_e ($\theta_{e,\,up}$) with a threshold defined on the maximum surface θ_e ($\theta_{e,\,surf}$) observed at the same time, within a circle of radius 2.5° centred on the cyclone's pressure minimum. The 2.5° radius results from a sensitivity analysis reported in Supplementary S1. The SII at each location and time is defined as:

$$SII(x,t) = \theta_{e,\,up}(x,t) - \max \theta_{e,\,surf}(t) \tag{1}$$

The circle over which SII is computed excludes an inner circle of radius 0.6° (2.5 grid points) around the centre, to account for the fact that the eye generally displays the highest values of $\theta_{e,\,surf}$ but does not contribute to convection over the cyclone's evolution; including it would bias the surface reference value. Furthermore, we excluded TCs that made landfall or underwent extratropical transition around the time of their peak intensity, as retaining them would risk spurious detections of stratospheric intrusion driven by a lower surface baseline rather than by a genuine upper-level signal. For the same reason, SII was computed only after a cyclone reached tropical storm intensity (i.e., 18 m/s): in weaker storms, the absence of a well-defined eye means that $\theta_{e,\,surf}$ may not be warm enough to distinguish a possible stratospheric signal from the rest of the upper-level environment. This choice implies the exclusion of tropical depressions from the analysis as well.

Cyclones were divided into SE-HWC-storms and non-SE-HWC-storms based on their SII values: if, before reaching peak intensity, a cyclone displayed one or more grid points where $SII > 0$ for at least two consecutive timesteps (i.e., at least 12 hours), it was assigned to the SE-HWC-storms class; otherwise, to the non-SE-HWC-storms one.

2.3 SE-HWC frequency across intensity scales

The frequency of SE-HWC-storms was evaluated against their peak intensity (i.e., the maximum wind speed achieved by the storm) and the PI of TCs, the latter computed following Emanuel's formula [32], to assess the existence of relationships between SE-HWC formation and these two variables. The TC intensity of the population was divided into bins of 5 m/s, and the number of SE-HWC-storms, y_i, was counted for each bin i. The Cochran-Armitage test for trend [33] was applied to the resulting distribution by computing

$$z = \frac{\sum_i y_i(x_i - \overline{x})}{\sqrt{\overline{p}(1-\overline{p})\sum_i \sigma_i^2}}$$

where n_i is the total number of TCs in bin, x_i is the bin score (i.e., the bin midpoint), $\overline{x} = \frac{1}{N}\sum_i n_i x_i$ is the n_i-weighted mean of the bin scores for N elements, $\overline{p} = \frac{1}{N}\sum_i y_i$ is the pooled proportion of SE-HWC-storms across all bins, and σ_i^2 is defined as:

$$\sigma_i^2 = n_i(x_i - \overline{x})^2$$

Assuming that z is normally distributed, we compute the corresponding p-value, allowing us to test, at the 5% significance level, the null hypothesis that SE-HWC-storms occur with constant frequency across bins.

2.4 Statistical analysis

To set a common starting point for both TC classes, we restricted the analysis of all variables to the time span between the first timestep at which a cyclone reaches tropical storm intensity (TS time) and the time at which it reaches peak intensity (peak time). TS time sets a common starting point for all storms, as some might have been detected at a later stage of cyclogenesis than others, while peak time limits the analysis to cases where stratospheric intrusions might have affected the intensification process.

Variables extracted from IBTrACS are defined as single values at each timestep for each storm. In ERA5, we extracted a snapshot centred on the cyclone centre and computed the spatial mean of each snapshot over domains of different sizes, depending on the variable considered. To test whether SE-HWC-storms display specific characteristics, we computed the difference between the class medians of each variable (hereafter, the "observed difference", *obs*). We preferred the use of medians instead of distribution means as some of the variables analysed have skewed distributions.

The significance of the observed differences was assessed through a permutation test. We divided the maxima into subsets by year and by basin (North Atlantic, Eastern and Western Pacific, and Northern Indian Ocean + Southern hemisphere, the latter obtained by merging the Northern Indian basin owing to its otherwise limited sample size). At each iteration, we randomly shuffled the "SE-HWC-storms" and "non-SE-HWC-storms" labels among TCs that developed within the same basin and year, preserving the observed proportion between the two classes in each subset. Once this operation was completed for all basins and years, we computed the difference between the class medians of the variable of interest ($\overline{x}$). Repeating this operation a large number of times (i.e., $N_{tot} = 10^4$) allows the reconstruction of the probability distribution of the difference between medians under the null hypothesis of random label assignment. The empirical p-value for the observed difference was calculated as the fraction of iterations returning an absolute difference at least as large as the absolute observed difference:

$$p = \frac{N_{perm}(\overline{x} \mid |\overline{x}| > |obs|)}{N_{tot}}$$

Observed differences were deemed significant beyond the 99% confidence interval.

Analysed variables from IBTrACS include:

- Elapsed time from TS to peak time.
- Minimum distance to land and distance to land at peak intensity.

The latter was analysed to gather information on possible causes of the storm's dissipation.

Variables computed from ERA5 are:

- PI, computed following Emanuel's formula [32] and averaged over an annulus centred on the TC, with internal and external radii $r_{int} = r_{max}(t) - 0.25°$ and $r_{ext} = r_{max}(t) + 0.25°$, respectively, where $r_{max}(t)$ is the storm's radius of maximum wind at each timestep. r_{max} was extracted from IBTrACS and, when unavailable, linearly interpolated from available data or, failing that, assumed to be 1° from the TC centre.
- Normalized intensity, defined as the ratio between maximum wind speed attained by the storm and its PI.
- SST, computed as the spatial average over 4°×4° square snapshots centred on the TC. Time-averaged SST is reported in Supplementary S3, while SST evaluated at time of maximum PI is reported in Supplementary S4.

- $\Delta k = k^*_{sst} - k_{2m}$, where $k^*_{sst} = c_p SST + L_v q^*(SST)$ and $k_{2m} = c_p T_{2m} + L_v q_{2m}$; c_p is the specific heat of air at constant pressure, L_v is the latent heat of vaporisation, $q^*(SST)$ is the saturation mixing ratio at the SST, and T_{2m} and q_{2m} are the air temperature and mixing ratio at 2 m. This variable was averaged over a 4°×4° square domain. Its value at time of maximum PI is reported in Supplementary S4.

- T_o, computed as the temperature of the equilibrium level and averaged over a 4°×4° square domain. The equilibrium level was retrieved by computing the moist adiabatic temperature profile from ERA5 data at 1° resolution and comparing it to the environmental temperature profile. The T_o value at time of maximum PI is reported in Supplementary S4.

- Vertical mass flux rate (F), computed at 200 hPa at the time of the storm as

$$F = -\int_{\Omega(x|\omega(x)<0)} \frac{\omega(x)}{g}\, dx$$

  where ω is the ERA5 pressure tendency (in Pa/s), g is the gravitational acceleration, x indicates a grid cell, and $\Omega(x|\omega(x) < 0)$ denotes the grid points, within an 8°×8° square domain centred on the TC, where the pressure tendency is upward.

- F increase rate, defined as the difference between the maximum value attained by F and its value at TS time, divided by the elapsed time between the two.

- Convective area, computed as the total area over which $\omega(x) < 0$ at a given time. We report in Supplementary S5 its value at the time of F_{max}.

- Mean mass flow, computed as the ratio between F and the convective area. It displays eventual differences in the increase of updraft intensity between the two classes. We report in Supplementary S5 its value at the time of F_{max}.

- High-level VWS, computed as the magnitude of the difference between the horizontal wind fields at 500 and 200 hPa, spatially averaged over an 8°×8° square centred on the TC. This shear layer was chosen as [3] showed it to be more closely related to TC dissipation than the "classical" 850-200 hPa shear. Unlike the other variables, VWS was additionally averaged over the whole TS-to-peak period for each track to account for the sustained detrimental effect of the environment on the TC, rather than an instantaneous value at a given time.

- Mid-tropospheric (i.e., at 600 hPa) specific humidity q, averaged over a 4°×4° square domain. Similarly to VWS, this variable was averaged over the TS-to-peak period.

We analysed the tropopause pressure from the coarse-grained dataset presented in [34] to identify an appropriate upper-tropospheric pressure level for this analysis. The dataset indicated that 200 hPa was a suitable choice for all cyclones and would prevent an overestimation of SII due to a lower tropopause height.

	Observed diff.	Null mean	p-value	Significant
Intensity-related variables				
v_{max} (m/s)	23.1	2.4	< 0.0001	✓
PI (m/s)	0.11	-0.08	0.61	✗
Normalized intensity (v_{max}/PI)	0.26	0.035	< 0.0001	✓
Mean SST (K)*	-0.30	0.02	< 0.0001	✓
SST at time of max PI (K)*	-0.16	0.03	< 0.0001	✓
Δk at time of max PI (J/kg)*	22.1	-42.0	0.67	✗
T_o at time of max PI (K)*	-0.44	-0.36	0.49	✗
Mass exchanges-related variables				
F at TS time (10^9 kg/s)*	1.5	0.72	0.029	✗
F_{max} (10^9 kg/s)	5.9	1.8	< 0.0001	✓
F increase rate (10^8 kg/s/day)	-7.0	-0.32	0.012	✗
Time to peak (days)	1.75	0.24	< 0.0001	✓
Convective area at time of F_{max} (10^9 m^2)*	4.1	1.0	< 0.0001	✓
Mean mass flux at time of F_{max} (10^{-3} kg s^{-1} m^{-2})*	7.3	2.2	< 0.0001	✓
Detrimental variables				
Time-averaged VWS (m/s)	-0.89	-0.01	< 0.0001	✓
Mid-tropospheric specific humidity q (g/kg)	0.19	0.04	< 0.0001	✓
Minimum distance to land (km)	337.5	30.4	< 0.0001	✓

Table 1: Differences between median values of TC-related metrics between the two cyclone classes. *Observed diff.* is the difference between the class medians (SE-HWC-storms minus non-SE-HWC-storms). *Null mean* is the mean difference of the empirical null distribution obtained from 10^4 label permutations, stratified per each year and basin. The significance of the difference between the two classes is evaluated through a two-sided p-value test. The last column indicates significance at 99% confidence level (✓: significant, ✗: not significant). Histograms of the variables marked with an asterisk are shown in the Supplementary Information.

References

1. Cangialosi, J. P. *et al.* Recent Progress in Tropical Cyclone Intensity Forecasting at the National Hurricane Center. *Weather and Forecasting* **35,** 1913–1922. ISSN: 0882-8156 (5 Oct. 2020).
2. Xu, J. & Wang, Y. Dependence of Tropical Cyclone Intensification Rate on Sea Surface Temperature, Storm Intensity, and Size in the Western North Pacific. *Weather and Forecasting* **33,** 523–537. ISSN: 0882-8156 (2 Apr. 2018).
3. Fu, H., Wang, Y., Riemer, M. & Li, Q. Effect of Unidirectional Vertical Wind Shear on Tropical Cyclone Intensity Change—Lower-Layer Shear Versus Upper-Layer Shear. *Journal of Geophysical Research: Atmospheres* **124,** 6265–6282. eprint: `https://agupubs.onlinelibrary.wiley.com/doi/pdf/10.1029/2019JD030586`. `https://agupubs.onlinelibrary.wiley.com/doi/abs/10.1029/2019JD030586` (2019).
4. Kossin, J. P. & Sitkowski, M. Predicting hurricane intensity and structure changes associated with eyewall replacement cycles. *Weather and forecasting* **27,** 484–488 (2012).
5. Schubert, W. H. & Hack, J. J. Inertial stability and tropical cyclone development. *Journal of Atmospheric Sciences* **39,** 1687–1697 (1982).
6. Hart, R. E. A Cyclone Phase Space Derived from Thermal Wind and Thermal Asymmetry. *Monthly Weather Review* **131,** 585–616. `https://journals.ametsoc.org/view/journals/mwre/131/4/1520-0493_2003_131_0585_acpsdf_2.0.co_2.xml` (2003).

7. Komaromi, W. A. & Doyle, J. D. Tropical Cyclone Outflow and Warm Core Structure as Revealed by HS3 Dropsonde Data. *Journal of the Atmospheric Sciences* **74,** 1339–1359 (2017).

8. Zhang, D. L. & Chen, H. Importance of the upper-level warm core in the rapid intensification of a tropical cyclone. *Geophysical Research Letters* **39.** ISSN: 00948276 (2 Jan. 2012).

9. Ohno, T. & Satoh, M. On the warm core of a tropical cyclone formed near the tropopause. *Journal of the Atmospheric Sciences* **72,** 551–571. ISSN: 15200469 (2 2015).

10. Kieu, C., Tallapragada, V., Zhang, D. L. & Moon, Z. On the development of double warm-core structures in intense tropical cyclones. *Journal of the Atmospheric Sciences* **73,** 4487–4506. ISSN: 15200469 (11 2016).

11. Moon, Z. & Kieu, C. Impacts of the lower stratosphere on the development of intense tropical cyclones. *Atmosphere* **8.** ISSN: 20734433 (7 July 2017).

12. Polesello, A., Charinti, G. A., Meroni, A. N., Muller, C. J. & Pasquero, C. Intensity Oscillations of Tropical Cyclones: Surface Versus Mid and Upper Tropospheric Processes. *Journal of Advances in Modeling Earth Systems* **17.** ISSN: 1942-2466 (4 Apr. 2025).

13. Charinti, G. A., Davin, A., Pasquero, C. & Muller, C. Impact of upper-level warming on tropical cyclone intensity. *Geophysical research letters* (2026).

14. Davin, A., Charinti, G. A., Muller, C., Polesello, A. & Pasquero, C. Stratospheric influence on tropical cyclone evolution. *Quarterly Journal of the Royal Meteorological Society* **n/a,** e70280. eprint: `https://rmets.onlinelibrary.wiley.com/doi/pdf/10.1002/qj.70280`. `https://rmets.onlinelibrary.wiley.com/doi/abs/10.1002/qj.70280` (2026).

15. Stohl, A. *et al.* Stratosphere-troposphere exchange: A review, and what we have learned from STACCATO. *Journal of Geophysical Research: Atmospheres* **108.** eprint: `https://agupubs.onlinelibrary.wiley.com/doi/pdf/10.1029/2002JD002490`. `https://agupubs.onlinelibrary.wiley.com/doi/abs/10.1029/2002JD002490` (2003).

16. Allison, T., Fuelberg, H. & Heath, N. Simulations of vertical water vapor transport for TC Ingrid (2013). *Journal of Geophysical Research: Atmospheres* **123,** 8255–8282 (2018).

17. Preston, A. D., Fuelberg, H. E. & Barth, M. C. Simulation of chemical transport by Typhoon Mireille (1991). *Journal of Geophysical Research: Atmospheres* **124,** 11614–11639 (2019).

18. Jiang, B., Lin, W., Hu, C. & Wu, Y. Tropical cyclones impact on tropopause and the lower stratosphere vapour based on satellite data. *Atmospheric Science Letters* **21.** ISSN: 1530261X (12 Dec. 2020).

19. Fagan, H. E. & Homeyer, C. R. Upper troposphere lower stratosphere composition change in tropical cyclones: Assessments from 17 years of satellite observations. *Journal of Geophysical Research: Atmospheres* **130,** e2025JD044717 (2025).

20. Leclair De Bellevue, J., Réchou, A., Baray, J.-L., Ancellet, G. & Diab, R. Signatures of stratosphere to troposphere transport near deep convective events in the southern subtropics. *Journal of Geophysical Research: Atmospheres* **111** (2006).

21. Ratnam, M. V. *et al.* Effect of tropical cyclones on the stratosphere-troposphere exchange observed using satellite observations over the north Indian Ocean. *Atmospheric Chemistry and Physics* **16,** 8581–8591. ISSN: 16807324 (13 July 2016).

22. Rodgers, E. B., Stout, J., Steranka, J. & Chang, S. Tropical Cyclone-Upper Atmospheric Interaction as Inferred from Satellite Total Ozone Observations. *Journal of Applied Meteorology and Climatology* **29,** 934–954. `https://journals.ametsoc.org/view/journals/apme/29/9/1520-0450_1990_029_0934_tcuaia_2_0_co_2.xml` (1990).

23. Wang, H. & Wang, Y. A Numerical Study of Typhoon Megi (2010). Part I: Rapid Intensification. *Monthly Weather Review* **142,** 29–48. https://journals.ametsoc.org/view/journals/mwre/142/1/mwr-d-13-00070.1.xml (2014).

24. Knapp, K. R., Kruk, M. C., Levinson, D. H., Diamond, H. J. & Neumann, C. J. The International Best Track Archive for Climate Stewardship (IBTrACS): Unifying Tropical Cyclone Data. *Bulletin of the American Meteorological Society* **91,** 363–376 (2010).

25. Hersbach, H., Bell, B., Berrisford, P., *et al.* The ERA5 global reanalysis. *Quarterly Journal of the Royal Meteorological Society* **146,** 1999–2049 (2020).

26. Tang, B. & Emanuel, K. Sensitivity of tropical cyclone intensity to ventilation in an axisymmetric model. *Journal of the Atmospheric Sciences* **69,** 2394–2413 (2012).

27. Grant, D. D. *et al.* Ozone transport by mesoscale convective storms in western Senegal. *Atmospheric Environment* **42,** 7104–7114. ISSN: 1352-2310. https://www.sciencedirect.com/science/article/pii/S1352231008005669 (2008).

28. Zhan, R. & Wang, Y. Contribution of tropical cyclones to stratosphere-troposphere exchange over the northwest Pacific: Estimation based on AIRS satellite retrievals and ERA-Interim data. *Journal of Geophysical Research: Atmospheres* **117** (2012).

29. Simmons, A. *et al.* Global stratospheric temperature bias and other stratospheric aspects of ERA5 and ERA5. 1 (2020).

30. Hodges, K., Cobb, A. & Vidale, P. L. How Well Are Tropical Cyclones Represented in Reanalysis Datasets? *Journal of Climate* **30,** 5243–5264 (2017).

31. Dauhut, T., Chaboureau, J.-P., Mascart, P. & Pauluis, O. The atmospheric overturning induced by Hector the Convector. *Journal of the Atmospheric Sciences* **74,** 3271–3284 (2017).

32. Emanuel, K. A. Sensitivity of Tropical Cyclones to Surface Exchange Coefficients and a Revised Steady-State Model incorporating Eye Dynamics. *Journal of the Atmospheric Sciences* **52,** 3969–3976. ISSN: 0022-4928 (22 Nov. 1995).

33. Armitage, P. Tests for Linear Trends in Proportions and Frequencies. *Biometrics* **11,** 375–386. ISSN: 0006341X, 15410420. http://www.jstor.org/stable/3001775 (2026) (1955).

34. Hoffmann, L. & Spang, R. An assessment of tropopause characteristics of the ERA5 and ERA-Interim meteorological reanalyses. *Atmospheric Chemistry and Physics* **22,** 4019–4046. https://acp.copernicus.org/articles/22/4019/2022/ (2022).

Supplementary Files

This is a list of supplementary files associated with this preprint. Click to download.

- SupplementaryERA5.pdf